RESEARCH ARTICLE

Removal of fluconazole from aqueous solution by magnetic biochar treated by ball milling: adsorption performance and mechanism

Zhexi Huang[1,2,3] · Yunqiang Yi[1,2,3] · Nuanqin Zhang[1,2] · Pokeung Eric Tsang[4] · Zhanqiang Fang[1,2,3]

Abstract

The problem of low adsorption capacity of pristine magnetic biochar for organic pollutants always occurs. It is of great significance to select a suitable method to improve the adsorption performance of magnetic biochar. In this study, magnetic biochar was treated by ball milling and tested for its fluconazole adsorption capacity. The maximum adsorption capacity of ball-milled magnetic biochar (BMBC) for fluconazole reached nearly 15.90 mg/g, which was approximately five times higher than that of pristine magnetic biochar (MBC). Fluconazole adsorption by BMBC was mainly attributed to π–π interactions, hydrogen bonding, and surface complexation with oxygen-containing functional groups. The enhancement in fluconazole adsorption by BMBC was attributed to an increase in oxygen-containing functional groups. Batch adsorption experiments also illustrated that BMBC could be successfully applied in a wide range of pH values. The high efficiency of fluconazole removal confirmed that ball milling was an effective strategy to enhance the adsorptive performance of magnetic biochar.

Keywords Magnetic biochar · Ball milling · Fluconazole · Adsorption mechanism · Oxygen-containing functional groups

Introduction

Magnetic biochar is usually derived from biomass and transition metal salts, and it has been confirmed as a high-efficiency adsorbent for typical pollutants (such as antibiotics, organic dyes, and heavy metals) in aqueous solution (Xu et al. 2020; Yi et al. 2019a; Li et al. 2020a; Liu et al. 2019). Magnetic biochar has the advantage that it can be recovered from the reaction medium by magnetic separation (Rocha et al. 2020; Hassan et al. 2020; Li et al. 2018a). Therefore,

✉ Yunqiang Yi
  20200582@m.scnu.edu.cn

1 School of Environment, South China Normal University, Guangzhou 510006, China

2 Guangdong Technology Research Center for Ecological Management and Remediation of Water System, Guangzhou 510006, China

3 Guangdong Provincial Key Laboratory of Chemical Pollution & Environmental Safety, Guangzhou 510006, China

4 Department of Science and Environmental Studies, The Education University of Hong Kong, Hong Kong 00852, China

environmental remediation technology based on magnetic biochar has been widely used.

Thus far, the methods used to synthesize magnetic biochar have mainly included impregnation–pyrolysis, the hydrothermal approach, and co-precipitation (Liang et al. 2019; Cai et al. 2018; Oladipo and Ifebajo 2017). However, irrespective of the method that is used to synthesize magnetic biochar, the adsorption performance of the unmodified product is limited. Therefore, metal element or metal oxide doping (Li et al. 2019; Jung et al. 2017), acid–base activation (Tang et al. 2018), organic functional group grafting (Li et al. 2018a, b, c; Zhou et al. 2018), and chemical oxidation (Xu et al. 2020) are generally used to enhance the adsorption performance of magnetic biochar. For instance, Li et al. (2018a, b, c) demonstrated that surface functional groups of magnetic biochar were enriched by chitosan modification, which significantly improved the material's adsorption capability for Cd(II). Meanwhile, the maximum adsorption capacity of Pb(II) by CeO_2-MoS_2-modified magnetic biochar was 263.6 mg/g, which was approximately 10 times higher than that of the original magnetic biochar (Li et al. 2019). However, despite their effectiveness in improving the adsorption performance of magnetic biochar, the methods mentioned above have some drawbacks, such as complex modification processes, high costs, and the use of toxic and

harmful substances. Therefore, it is necessary to identify a green and efficient method to enhance the adsorption performance of magnetic biochar.

Ball milling has been widely used to enhance surface area, reduce particle size, or enrich the surface functional groups of adsorbents, due to its advantages of simple operation, high efficiency, and low cost (Zhuang et al. 2021; Kumar et al. 2020; Zhang et al. 2019a). Xiang et al. (2020) revealed that ball milling effectively enhanced the specific surface area of biochar. They also showed that the adsorption capacity of ball-milled biochar for tetracycline was three times higher than that of pristine biochar. Similarly, Li et al. (2020b) revealed that magnetic biochar was transformed into magnetic nanobiochar using ball milling, which significantly enhanced the adsorption capacity of magnetic biochar for tetracycline and Hg(II). Therefore, it is theoretically feasible to improve the adsorption performance of magnetic biochar by ball milling.

Fluconazole is a broad-spectrum antifungal drug, which has been detected as a pollutant in water bodies (Assress et al. 2020, 2019). Residual fluconazole poses a great threat to aquatic ecological environments (Zhang et al. 2020; Richter et al. 2016). Therefore, it is of great significance to eliminate fluconazole from wastewater. In this study, ball-milled magnetic biochar was prepared and used for fluconazole adsorption. The following items were investigated: (1) the physicochemical properties of ball-milled magnetic biochar; (2) the adsorption kinetics and adsorption isotherms of fluconazole by ball-milled magnetic biochar; (3) the adsorption mechanism of fluconazole by ball-milled magnetic biochar; and (4) the influence of pH, humic acid, and biomass type on the adsorption of fluconazole by ball-milled magnetic biochar.

Materials and methods

Reagents

Fluconazole (analytical purity), ferrous sulfate heptahydrate ($FeSO_4 \cdot 7H_2O$; analytical purity), sodium hydroxide (superior purity), ammonium formate, and acetonitrile were purchased from Energy Chemical Reagent Company, China. Hydrochloric acid (HCl; analytical purity) was purchased from Guangzhou Chemical Reagent Factory, China.

Material preparation

Ten grams of rice husk was mixed in 30 mL of dilute HCl (0.1 mol/L) for 6 h to remove impurities. This pretreated rice husk was added to 100 mL of Fe^{2+} solution (1.2 g/L) and stirred for 24 h. Subsequently, the mixture was centrifuged, and the residue was placed in a muffle furnace for 1.5 h at

a pyrolysis temperature of 600℃ in a nitrogen atmosphere. Finally, after being milled and sieved to pass through a 100-mesh sieve, the obtained sample was labeled as pristine magnetic biochar (MBC). Subsequently, MBC (1 g) and steel balls were added into stainless steel vials and placed in a planetary ball mill (MBC to ball mass ratio = 1:100 (Zhang et al. 2019a, b); the mass ratio of 10-mm and 6-mm balls was 8:2). Ball milling was operated at 400 r/min for 24 h in ambient air conditions, and the direction of rotation was changed every 6 h. The obtained sample was labeled as ball-milled magnetic biochar (BMBC).

Material characterization

A surface analyzer (ASAP2020M; USA) was used to measure the specific surface area and pore size distribution of MBC and BMBC. The surface morphology of MBC and BMBC was investigated using scanning electron microscopy (SEM; Tuscan mira3, Germany) equipped with energy-dispersive X-ray spectroscopy (Oxford X-MAX, UK). Fourier-transform infrared spectroscopy (FT-IR; Horiba, Emax, Japan) was conducted to obtain information on the surface functional groups of MBC and BMBC. The phase structures of MBC and BMBC were analyzed by X-ray diffraction (D8 advance, Bruker, Germany). The valence states of elements on the surface of BMBC were measured by X-ray photo-electron spectroscopy (XPS; ESCALAB 250; Thermo-VG Scientific, USA). The magnetic properties of BMBC were determined with a comprehensive physical measurement system (PPMS-9; Quantum Design, USA). The carbon (C), hydrogen (H), nitrogen (N), and oxygen (O) contents of BMBC were determined using an elemental analyzer (varia EL CUBE, Germany).

Adsorption experiments

For adsorption kinetic experiments, BMBC (1 g/L) was added to a conical flask containing 100 mL of fluconazole solution (20 mg/L, pH = 5.6). The flasks were shaken in a thermostatic oscillator (200 r/min, 30 °C ± 0.5 ℃). At the pre-selected time, the suspensions were immediately filtered through chemical analytical filter paper. The remaining fluconazole in the solutions was measured by high-performance liquid chromatography. Detailed testing methods are shown in our previous studies (Zhang et al. 2020). The removal efficiency of fluconazole was calculated using the following equation:

$$\eta = \frac{C_0 - C_e}{C_0} \times 100\% \tag{1}$$

where C_0 and C_e are the initial and equilibrium concentrations of fluconazole (mg/L), respectively.

The equilibrium adsorption capacity was calculated using the following equation:

$$Q_e = \frac{(C_0 - C_e)\text{x}V}{W} \tag{2}$$

where Q_e is the adsorption capacity (mg/g), C_0 and C_e are the initial and equilibrium concentrations of fluconazole in the solution, and V and W are the volume of solution (mL) and the dosage of BMBC (g/L), respectively.

The data for adsorption kinetics were fitted by the pseudo-first-order (Eq. 3), pseudo-second-order (Eq. 4), and Elovich (Eq. 5) models, respectively. The kinetic models are represented as:

$$Q_t = Q_e\left(1 - e^{-k_1 t}\right) \tag{3}$$

$$\frac{t}{Q_t} = \frac{1}{Q_e}t + \frac{1}{k_2 Q_e^2} \tag{4}$$

$$Q_t = \alpha + \beta \ln t \tag{5}$$

where Q_e represents the adsorption capacity of fluconazole at equilibrium, Q_t (mg/g) is the adsorption capacity for fluconazole at time t, and k_1 and k_2 are the pseudo-first-order rate constant (min^{-1}) and the pseudo-second-order rate constant (g/mg/min), respectively. α is the initial adsorption rate (mg/kg), and β is the desorption constant (kg/mg).

For adsorption isotherm measurement, BMBC was placed into a conical flask containing 100 mL of solution of different concentrations of fluconazole (5, 10, 15, 20, 25, and 30 mg/L). The mixture was shaken for 6 h at different temperatures (20 °C ± 0.5 °C, 30 °C ± 0.5 °C, and 40 °C ± 0.5 °C). The experimental data were fitted using the Langmuir (Eq. 6) and Freundlich (Eq. 7) models as follows:

$$\frac{C_e}{Q_e} = \frac{1}{K_L Q_m} + \frac{C_e}{Q_m} \tag{6}$$

$$Q_e = K_F C_e^{\frac{1}{n}} \tag{7}$$

where Q_m (mg/g) is the maximum adsorption capacity for fluconazole, K_L (L/mg) is the Langmuir isotherm constant, K_F (mg/g (L/mg)^n) is the Freundlich isotherm constant, and n is the measure of adsorption intensity.

The thermodynamic parameters, including standard free energy change (ΔG), standard enthalpy change (ΔH), and standard entropy change (ΔS), were calculated using Eqs. 8 and 9 as follows:

$$\Delta G = -RT \ln K \tag{8}$$

$$\ln K = \Delta S/R - \Delta H/(RT) \tag{9}$$

where K is the adsorption equilibrium constant, T (K) is the absolute temperature, and R (8.314 J/mol/K) is the gas constant. ΔH and ΔS could be calculated from the slope and intercept of ln K versus 1/T.

Finally, the influences of pH, humic acid, and biomass species on the adsorption of fluconazole by BMBC were investigated. Each experiment was conducted in duplicate.

Results and discussion

Material characterization

The structure and phase compositions of MBC and BMBC were observed by XRD (Fig. S1 (a)). For MBC, the broad diffraction peaks at 20°–30° are generally considered to represent silica, graphitic carbon, and amorphous iron oxides (Huang et al. 2020; Zhong et al., 2018). The peak at 44.3° corresponded to the (110) plane of Fe^0 in MBC, and the (220), (100), and (440) planes of Fe$_3$O$_4$ were also observed in MBC. After ball milling, the (100) plane of Fe$_3$O$_4$ and the (110) plane of Fe^0 were strengthened, indicating that ball milling was beneficial to the crystallinity of Fe$_3$O$_4$ and Fe^0 in MBC. Meanwhile, the saturation magnetization of BMBC (Fig. S1 (b)) was 55.15 emu/g, which was nearly 2.38 times higher than that of MBC. The above results provide evidence that ball milling improved the crystallinity of iron and iron oxides in the MBC and alignment of the magnetic domains in the crystal structure (Fu et al. 2019).

SEM images (Fig. 1) revealed that MBC exhibited an abundant porous structure, and iron oxides adhered to the surface of MBC. After ball milling, the pore structure of BMBC disappeared. Additionally, the particles of iron oxides in BMBC were significantly reduced in size, and most of them approached the nanoscale. The results of element mapping (Fig. 2) suggested that Fe, C, and O were evenly distributed on the surface of BMBC. The specific surface area of MBC (Fig. S2 (a)) was 211.18 m^2/g, whereas that of BMBC was reduced by a factor of 1.69. The above results were possibly attributable to the pore structure of MBC being destroyed by ball milling, which is consistent with the results of SEM.

Surface functional groups of MBC and BMBC are presented in Fig. S2 (b). The peak at 3429 cm^{-1} was considered to be due to the stretching vibration of O–H (Zou et al. 2021). The peak at 1617 cm^{-1} represented the vibration of aromatic C = C and C = O (Wang et al. 2019). The vibration of –C–O–C appeared at 1099 cm^{-1} (Zhang et al. 2018). The peak at 805 cm^{-1} was attributed to the vibration of C–H in pyridine or furan, which are heterocyclic compounds (Wang et al. 2019). A peak at 469.1 cm^{-1} was assigned to the stretching of Si–O (Zhou et al. 2018). The results of
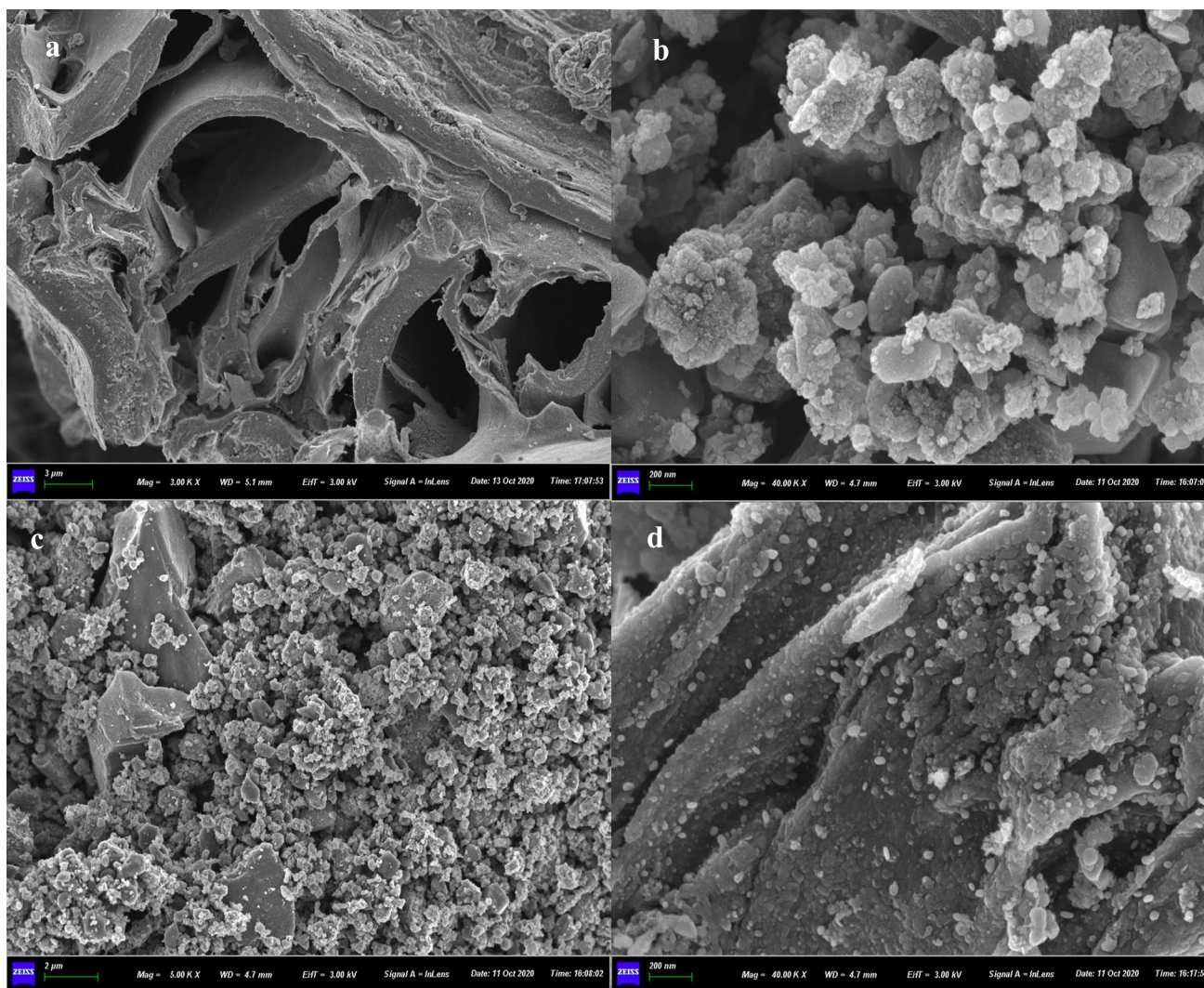
Fig. 1 Scanning electron microscopy images of pristine magnetic biochar (**a**, **b**) and ball-milled magnetic biochar (**c**, **d**)

FT-IR demonstrate that ball milling had little effect on the surface functional groups of magnetic biochar.

XPS spectra of MBC and BMBC are indicated in Fig. 3. Three diffraction peaks of C, O, and Fe were observed in MBC and BMBC. The Fe2p spectra of MBC and BMBC could be deconvoluted into three peaks of Fe^0(707 eV), Fe(II) (710.0 and 724.0 eV), and Fe(III) (712.0 and 726.3 eV) (Jiang et al. 2019a; Zhang et al. 2018; Yang et al. 2016). Compared with MBC, the characteristic peak of Fe^0 in BMBC decreased slightly, indicating that ball milling reduced the content of Fe^0 in MBC. In addition, the intensity ratio of Fe(II)/Fe(III) in MBC decreased from 1.7 to approximately 0.9 after ball milling, demonstrating that Fe(II) was oxidized during ball milling. The O1s spectra of the materials showed binding energies of 531.1–531.8, 532.2–533.3, and 534.0–535.4 eV, which corresponded to –C=O, –C–O, and –OH groups, respectively (Jiang et al. 2019b; Zhou

et al. 2017). It is worth mentioning that compared with MBC, the content of –OH groups in BMBC decreased significantly, while the proportion of –C=O increased significantly. In the C1s spectra, the binding energies of 284.0, 284.5, and 285.0 eV corresponded to –C=C/–C–C, –C–O, and –C=O groups, respectively (Reguyal and Sarmah 2018; Ahmed et al. 2017). The relative content of –C=O increased after ball milling, implying that ball milling could significantly increase the content of –C=O functional groups in MBC.

The elemental compositions of MBC and BMBC are listed in Table 1. In BMBC, the content of C was lower than that in MBC, while the contents of H, O, and N were higher. In addition, the O/C, H/C, and (N+O)/C values of the magnetic biochar increased after ball milling, suggesting that ball milling reduces the hydrophobicity and improves the polarity of magnetic biochar.

Fig. 2 Element mapping of ball-milled magnetic biochar (**a**), carbon mapping of ball-milled magnetic biochar(**b**), oxygen mapping of ball-milled magnetic biochar(**c**), and iron mapping of ball-milled magnetic biochar(**d**)
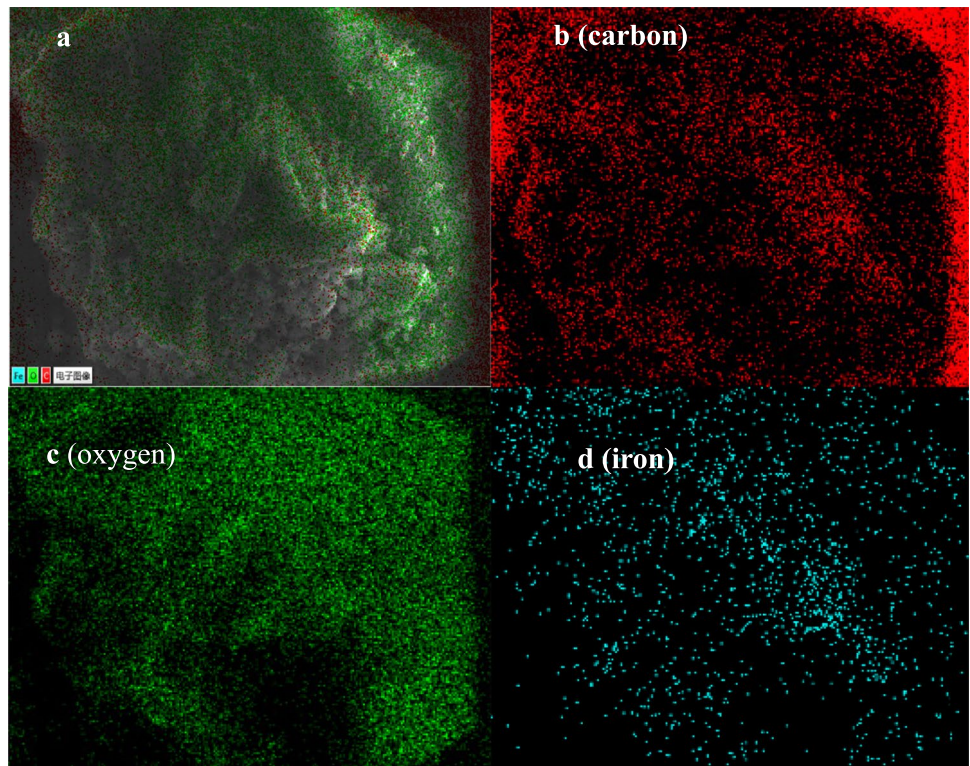
Fig. 3 X-ray photoelectron spectra (**a**), Fe2p spectra (**b**), O1s spectra (**c**), and C1s spectra (**d**)
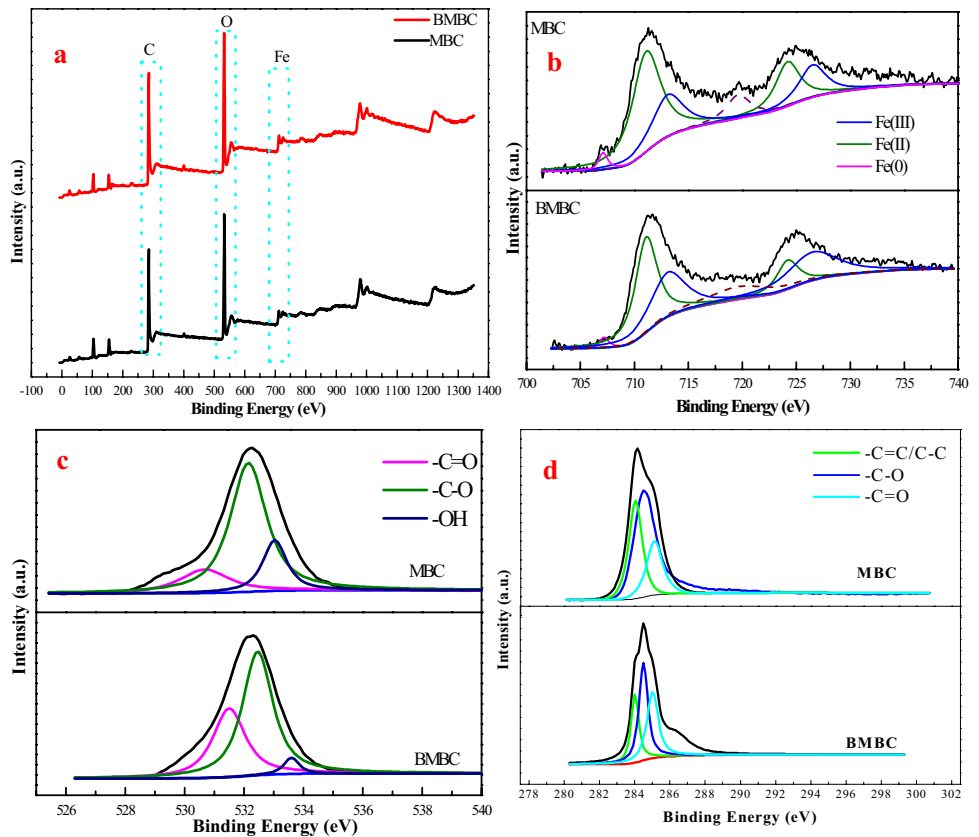
Table 1 Element analysis of pristine magnetic biochar (MBC) and ball-milled magnetic biochar (BMBC)

Material	Element analysis (%)				Atomic ratio		
	N	C	H	O	O/C	H/C	(N+O)/C
MBC	0.79	31.33	0.892	11.06	0.26	0.34	0.29
BMBC	0.76	28.22	1.656	21.69	0.58	0.70	0.60

Adsorption of fluconazole by MBC and BMBC

The adsorption kinetics of fluconazole by MBC and BMBC are shown in Fig. 4a. Although MBC and BMBC had different adsorption capacities for fluconazole, both reached adsorption equilibrium within approximately 6 h. The equilibrium adsorption capacity of BMBC for fluconazole was nearly 13.5 mg/g, which was approximately three times that of MBC. Furthermore, the fitting results of the three adsorption kinetic models are shown in Table S1. The correlation coefficient (R^2) of the Elovich model was > 0.99, which was greater than that of the pseudo-first-order and pseudo-second-order kinetic models, indicating that fluconazole adsorption by BMBC mainly occurs by chemical adsorption (Han et al. 2016; Zhang et al. 2013).

The experimental data were fitted by the Langmuir and Freundlich models (Fig. 4b), and the adsorption model parameters are listed in Table S2. With an increasing concentration of fluconazole, the adsorption capacity of the magnetic materials for fluconazole increased and gradually reached adsorption equilibrium. For MBC, the correlation coefficient of the Freundlich model was lower than that of the Langmuir model, illustrating that the adsorption of fluconazole by MBC was dominated by monolayer physical adsorption, and the adsorption capacity of MBC for fluconazole increased with an increase in reaction temperature. In contrast, the adsorption of fluconazole by BMBC was consistent with the Freundlich model, which may be attributable to the change in particle size and the surface structure of magnetic biochar caused by ball milling. In addition, $1/n$ is generally considered to be related to adsorption strength. For BMBC, the $1/n$ value decreased with an increase in

temperature, but remained between 0.3 and 0.4, indicating that BMBC had a strong adsorption capacity for fluconazole (Yan et al. 2015). Finally, according to the Langmuir fitting data, the adsorption capacity of BMBC for fluconazole was higher than that of MBC, which again showed that ball milling could effectively improve the adsorption performance of magnetic biochar.

The main adsorption thermodynamic parameters are provided in Table S3. The ΔG values were negative at all three temperatures for both MBC and BMBC, suggesting that adsorption was feasible and spontaneous (Jung et al. 2017). The absolute values of ΔG indicated that the driving force of adsorption for BMBC was higher than for MBC. The positive ΔS values revealed that fluconazole adsorption by MBC or BMBC was random rather than orderly (Yan et al. 2015). The ΔH values of BMBC and MBC indicate that the adsorption process was endothermic. The ΔH value of BMBC was nearly two times higher than that of MBC, showing that the endothermicity was increased (Jung et al. 2017; Yan et al. 2015).

Mechanism of fluconazole adsorption by BMBC

The XPS spectrum (Fig. 5) illustrates that the main components of spent BMBC were C, Fe, and O, and the peaks of O and C functional groups changed after BMBC was used (Table S4). Specifically, the binding energy of –C=C/–C–C shifted from 284.0 to 284.22 eV, that of –C–O shifted from 284.49 to 284.862 eV, and that of –C=O changed from 285.0 to 285.61 eV. Moreover, the relative content of these functional groups also changed after BMBC was used. For example, the relative content of –C=C/–C–C increased

Fig. 4 Adsorption kinetics (**a**) and adsorption isotherms (**b**) of fluconazole by pristine magnetic biochar (MBC) and ball-milled magnetic biochar (BMBC)
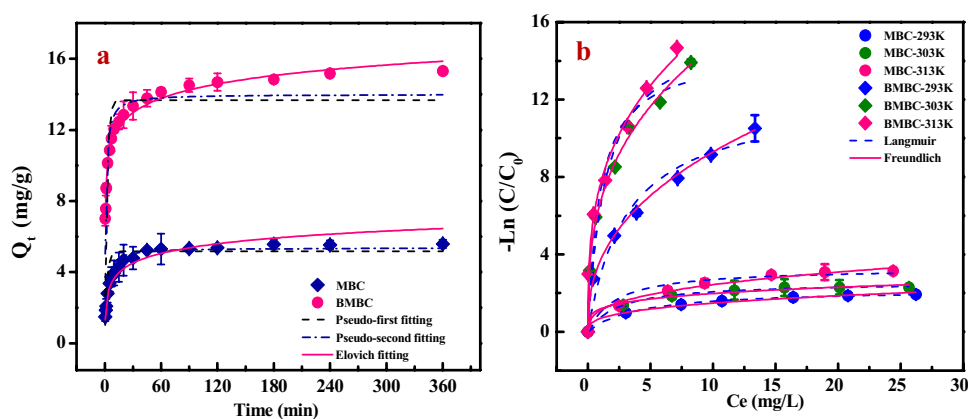
Fig. 5 X-ray photoelectron spectra (**a**), Fe2p (**b**), O1s (**c**), and C1s (**d**) spectra of spent ball-milled magnetic biochar
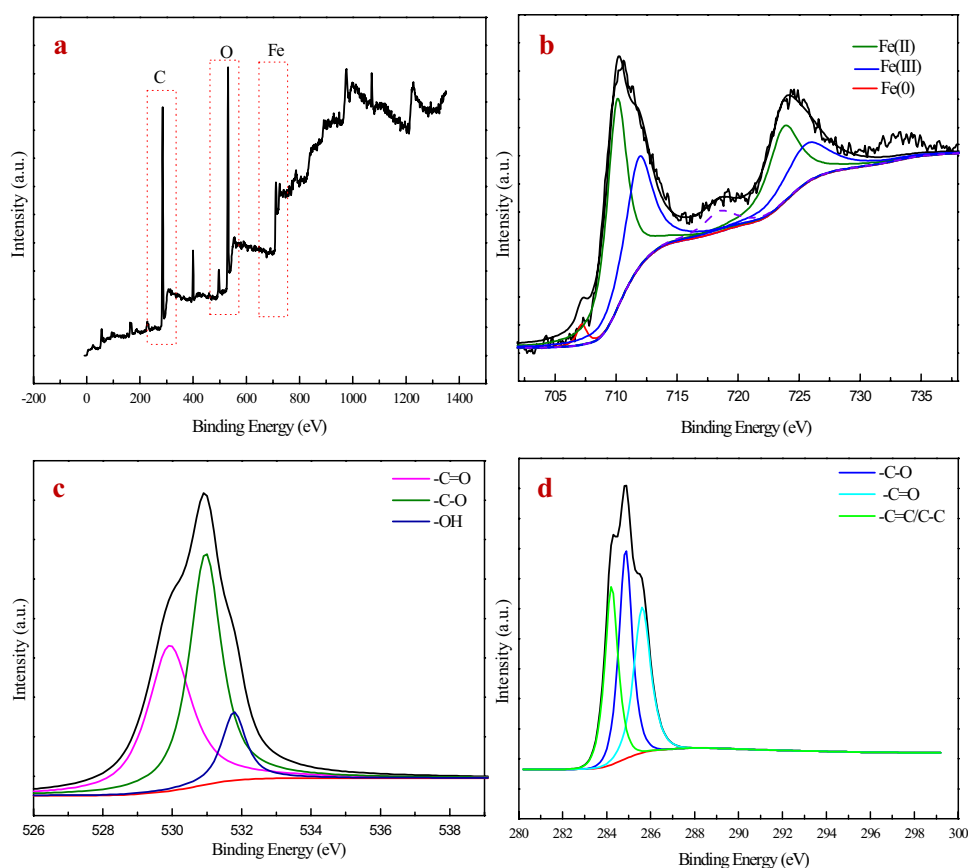
from 24.84 to 31.13%, indicating that fluconazole was successfully adsorbed by BMBC (Zhang et al. 2019b; Zhou et al. 2018). Conversely, the relative content of –C–O and –C=O in BMBC decreased, suggesting that these functional groups participated in fluconazole adsorption. The O1s spectrum also showed that the binding energy of O-containing functional groups in BMBC changed after the reaction. Specifically, the relative content of the functional group –C–O decreased from 55.97 to 48.05%, revealing that there was a chemical reaction between BMBC and fluconazole. Finally, from the Fe2p spectrum, it can be seen that the binding energy and content of Fe with different valence states changed only weakly after the reaction, indicating that Fe oxides in BMBC have little effect on fluconazole adsorption. Therefore, the C– and O-containing functional groups in BMBC contributed to fluconazole adsorption.

FT-IR (Fig. S3a) revealed no obvious difference in the infrared spectra of fresh and spent BMBC, illustrating that the types of functional groups in BMBC were unchanged. However, the peaks of some functional groups in BMBC shifted. For example, the peaks of aromatic C=C and C=O shifted from 1620.88 to 1618.15 cm^{-1}, the peaks of –C–O–C shifted from 1095.21 to 1097.95 cm^{-1}, and the peaks of C–H shifted from 802.73 to 806.77 cm^{-1}. This confirms that the functional groups in BMBC participated in fluconazole

adsorption (Li et al. 2018c; Ahmed et al. 2017). The results of XRD (Fig. S3b) illustrated that the phase composition and crystal structure of BMBC were relatively unaffected in the process of fluconazole adsorption, providing further evidence that Fe oxides, silica, and other components in BMBC contributed less to fluconazole adsorption. Finally, the results of SEM, specific surface area, and the effect of pH on fluconazole adsorption by BMBC (Fig. S4) identified that the contributions to pore-filling and electrostatic interaction on fluconazole adsorption were negligible.

Based on the above analysis, the mechanism of fluconazole adsorption by BMBC can be summarized as follows (Fig. 6): (1) The aromatic structure of fluconazole makes it a π-electron acceptor; meanwhile, the results of XRD show that the BMBC had a graphite-like structure. Therefore, π–π electron donor–acceptor interactions were responsible for fluconazole adsorption; (2) the results of XPS and FT-IR illustrate that fluconazole adsorption was also attributable to H bonding; (3) O-containing functional groups in BMBC complexed with fluconazole, which also contributed to fluconazole adsorption; (4) the pore-filling and hydrophobic effects had little contribution to fluconazole adsorption by BMBC. Therefore, π–π interactions, H bonding, and the complexation of O-containing functional groups were the main contributors to fluconazole adsorption, and the increase
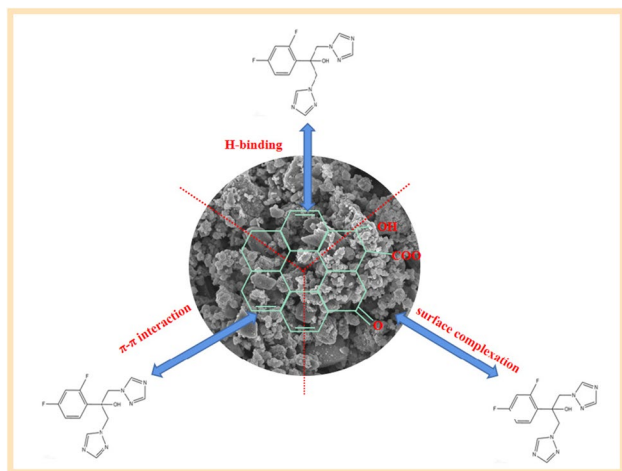
Fig. 6 The adsorption mechanism of fluconazole by BMBC

in O-containing functional groups was the key reason for the improvement in fluconazole adsorption by BMBC.

Influence of pH, humic acid, and biomass type on fluconazole adsorption by BMBC

Effects of pH

The influence of pH on fluconazole adsorption by BMBC is shown in Fig. S4. Acidic conditions were slightly more conducive to fluconazole adsorption, and the maximum adsorption capacity reached 13.5 mg/g at pH = 3.0. With an increase in pH, the adsorption capacity of BMBC for fluconazole decreased. However, even at pH = 11.0, the adsorption capacity of BMBC for fluconazole only decreased by 3.3 mg/g, indicating that BMBC has better pH shock resistance, and will undoubtedly have good practical application prospects.

Effects of humic acid

Humic acid commonly exists in water bodies. Previous studies have confirmed that the presence of humic acid can significantly affect the adsorption of target pollutants by adsorbents (Yang et al. 2017; Lian et al. 2015). Therefore, it is necessary to explore the effect of coexisting humic acid on fluconazole adsorption by BMBC. The effect of humic acid on fluconazole adsorption by BMBC is shown in Fig. S5. With the increase in humic acid concentration, the capacity of BMBC to adsorb fluconazole decreased only slightly, reaching 12.4 mg/g when the concentration of humic acid was 30 mg/L, which was only 1.4 mg/g lower than that of the system without humic acid. This illustrated that the influence of humic acid on fluconazole adsorption by BMBC was weak.

Effect of biomass type

The performance of magnetic biochar is closely related to the type of biomass from which it is prepared (Yi et al. 2019b). The influence of biomass type on fluconazole adsorption by MBC and BMBC is shown in Fig. S6. The best adsorption capacity for fluconazole (nearly 3 mg/g) was observed with the magnetic biochar prepared from rice husk, while the fluconazole adsorption capacity of magnetic biochar synthesized from wheat straw was lowest (< 1.5 mg/g). However, no matter what type of biomass was used as a raw material to synthesize magnetic biochar, the adsorption capacity for fluconazole significantly improved after ball milling and ranged from 3 to 11 times that of magnetic biochar without ball milling. These results show that the benefits of ball milling are effective for all types of magnetic biochar.

Conclusion

In this paper, magnetic biochar was prepared by impregnation–pyrolysis and treated by ball milling. Ball milling effectively improved the adsorption rate and capacity of magnetic biochar for fluconazole. The mechanism of fluconazole adsorption by BMBC included π–π interactions, H bonding, and complexation with O-containing functional groups. Batch experiments for fluconazole adsorption confirmed that BMBC was applicable across a wide range of pH and was resistant to interference. The results of fluconazole adsorption by BMBC from different biomass sources confirmed that ball milling is beneficial for different types of magnetic biochar.

Declarations

Ethics approval Not applicable.

Consent to participate The authors provided consent to participate in this study.

Consent for publication The authors provided consent to publish this study.

Competing interests The authors declare no competing interests.

References

Ahmed MB, Zhou JL, Ngo HH, Guo WS, Johir MAH, Sornalingam K, Belhaj D, Kallel M (2017) Nano-Fe^0 immobilized onto functionalized biochar gaining excellent stability during sorption and reduction of chloramphenicol via transforming to reusable magnetic composite. Chem Eng J 322:571–581. https://doi.org/10.1016/j.cej.2017.04.063

Assress HA, Nyoni H, Mamba BB, Msagati TAM (2019) Target quantification of azole antifungals and retrospective screening of other emerging pollutants in wastewater effluent using UHPLC-QTOF-MS. Environ Pollut 253:655–666. https://doi.org/10.1016/j.envpol.2019.07.075

Assress HA, Nyoni H, Mamba BB, Msagati TAM (2020) Occurrence and risk assessment of azole antifungal drugs in water and wastewater. Ecotoxicol Environ Saf 187:109868. https://doi.org/10.1016/j.ecoenv.2019.109868

Cai WQ, Wei JH, Li ZL, Liu Y, Zhou JB, Han BW (2018) Preparation of amino-functionalized magnetic biochar with excellent adsorption performance for Cr(VI) by a mild one-step hydrothermal method from peanut hull. Colloid Surf a 563:102–111. https://doi.org/10.1016/j.colsurfa.2018.11.062

Fu HC, Ma SL, Zhao P, Xu SJ, Zhan SH (2019) Activation of peroxymonosulfate by graphitized hierarchical porous biochar and MnFe$_2$O$_4$ magnetic nanoarchitecture for organic pollutants degradation: structure dependence and mechanism. Chem Eng J 360:157–170. https://doi.org/10.1016/j.cej.2018.11.207

Han YT, Cao X, Ouyang X, Sohi SP, Chen JW (2016) Adsorption kinetics of magnetic biochar derived from peanut hull on removal of Cr (VI) from aqueous solution: effects of production conditions and particle size. Chemosphere 145:336–341. https://doi.org/10.1016/j.chemosphere.2015.11.050

Hassan M, Naidu R, Du JH, Liu YJ, Qi FJ (2020) Critical review of magnetic biosorbents: their preparation, application, and regeneration for wastewater treatment. Sci Total Environ 702(134893):1. https://doi.org/10.1016/j.scitotenv.2019.134893

Huang DL, Zhang Q, Zhang C, Wang RZ, Deng R, Luo H, Li T, Li J, Chen S, Liu CH (2020) Mn doped magnetic biochar as persulfate activator for the degradation of tetracycline. Chem Eng J 391:123532. https://doi.org/10.1016/j.cej.2019.123532

Jiang SF, Ling LL, Chen WJ, Liu WJ, Li DC, Jiang H (2019a) High efficient removal of bisphenol A in a peroxymonosulfate/iron functionalized biochar system: mechanistic elucidation and quantification of the contributors. Chem Eng J 359:572583. https://doi.org/10.1016/j.cej.2018.11.124

Jiang SF, Xi KF, Yang J, Jiang H (2019b) Biochar-supported magnetic noble metallic nanoparticles for the fast recovery of excessive reductant during pollutant reduction. Chemosphere 227:63–71. https://doi.org/10.1016/j.chemosphere.2019.04.044

Jung KW, Lee S, Lee YJ (2017) Synthesis of novel magnesium ferrite (MgFe$_2$O$_4$)/biochar magnetic composites and its adsorption behavior for phosphate in aqueous solutions. Bioresource Technol 245:751–759. https://doi.org/10.1016/j.biortech.2017.09.035

Kumar M, Xiong XN, Wan ZH, Sun YQ, Tsang DCW, Gupta J, Gao B, Cao XD, Tang JC, Ok YS (2020) Ball milling as a mechanochemical technology for fabrication of novel biochar nanomaterials. Bioresource Technol 312:23613. https://doi.org/10.1016/j.biortech.2020.123613

Li MX, Liu HB, Chen TH, Dong C, Sun YB (2018a) Synthesis of magnetic biochar composites for enhanced uranium(VI) adsorption. Sci Total Environ 651:1020–1028. https://doi.org/10.1016/j.scitotenv.2018.09.259

Li RH, Deng HX, Zhang XF, Wang JJ, Awasthi MK, Wang Q, Xiao R, Zhou BY, Du J, Zhang ZQ (2019) High-efficiency removal of Pb(II) and humate by a CeO$_2$–MoS$_2$hybrid magnetic biochar. Bioresource Technol 273:335–340. https://doi.org/10.1016/j.biortech.2018.10.053

Li RH, Liang W, Huang H, Jiang SC, Guo D, Li ML, Zhang ZQ, Ali A, Wang JJ (2018b) Removal of cadmium(II) cations from an aqueous solution with aminothiourea chitosan strengthened magnetic biochar. J Appl Polym Sci 13519:46239. https://doi.org/10.1002/app.46239

Li RH, Zhang YC, Deng HX, Zhang ZQ, Wang JJ, Shaheen SM, Xiao R, Rinklebe J, Xi BD, He XS, Du J (2020a) Removing tetracycline and Hg(II) with ball-milled magnetic nanobiochar and its potential on polluted irrigation water reclamation. J Hazard Mater 384:121095. https://doi.org/10.1016/j.jhazmat.2019.121095

Li RN, Wang ZW, Zhao XT, Li X, Xie XY (2018c) Magnetic biochar-based manganese oxide composite for enhanced fluoroquinolone antibiotic removal from water. Environ Sci Pollut Res 25:31136–31148. https://doi.org/10.1007/s11356-018-3064-1

Li XP, Wang CB, Zhang JG, Liu JP, Liu B, Chen GY (2020b) Preparation and application of magnetic biochar in water treatment: a critical review. Sci Total Environ 711:134847. https://doi.org/10.1016/j.scitotenv.2019.134847

Lian F, Sun BB, Chen X, Zhu LY, Liu ZQ, Xing BS (2015) Effect of humic acid (HA) on sulfonamide sorption by biochars. Environ Pollut 204:306–312. https://doi.org/10.1016/j.envpol.2015.05.030

Liang J, Fang YL, Luo Y, Zeng GM, Deng JQ, Tan XF, Tang N, Li XM, He XY, Feng CT, Ye SJ (2019) Magnetic nanoferromanganese oxides modified biochar derived from pine sawdust for adsorption of tetracycline hydrochloride. Environ Sci Pollut Res 266:5892–5903. https://doi.org/10.1007/s11356-018-4033-4

Liu YY, Sohi SP, Liu SY, Guan JJ, Zhou JY, Chen JW (2019) Adsorption and reductive degradation of Cr(VI) and TCE by a simply synthesized zero valent iron magnetic biochar. J Environ Manage 235:276–281. https://doi.org/10.1016/j.jenvman.2019.01.045

Oladipo AA, Ifebajo AO (2017) Highly efficient magnetic chicken bone biochar for removal of tetracycline and fluorescent dye from wastewater: two-stage adsorber analysis. J Environ Manage 209:9–16. https://doi.org/10.1016/j.jenvman.2017.12.030

Reguyal F, Sarmah AK (2018) Site energy distribution analysis and influence of Fe$_3$O$_4$ nanoparticles on sulfamethoxazole sorption in aqueous solution by magnetic pine sawdust biochar. Environ Pollut 233:510–519. https://doi.org/10.1016/j.envpol.2017.09.076

Richter E, Roller E, Kunkel U, Ternes TA, Coors A (2016) Phytotoxicity of wastewater-born micropollutants-characterisation of three antimycotics and a cationic surfactant. Environ Pollut 208:512–522. https://doi.org/10.1016/j.envpol.2015.10.024

Rocha LS, Pereira D, Sousa E, Otero M, Esteves VI, Calisto V (2020) Recent advances on the development and application of magnetic activated carbon and char for the removal of pharmaceutical compounds from waters: a review. Sci Total Environ 718:137272. https://doi.org/10.1016/j.scitotenv.2019.134847

Tang L, Yu JF, Pang Y, Zeng GM, Deng YC, Wang JJ, Ren XY, Ye SJ, Peng B, Feng HP (2018) Sustainable efficient adsorbent: alkali-acid modified magnetic biochar derived from sewage sludge for aqueous organic contaminant removal. Chem Eng J 336:160–169. https://doi.org/10.1016/j.cej.2017.11.048

Wang SS, Zhao MY, Zhou M, Zhao YT, Li YC, Gao B, Feng K, Yin WQ, Ok YS, Wang XZ (2019) Biomass facilitated phase

transformation of natural hematite at high temperatures and sorption of Cd^{2+} and Cu^{2+}. Environ Int 124:473–481. https://doi.org/10.1016/j.envint.2019.01.004

Xiang W, Wan YS, Zhang XY, Tan ZZ, Xia TT, Zheng YL, Gao B (2020) Adsorption of tetracycline hydrochloride onto ball-milled biochar: governing factors and mechanisms. Chemosphere 255:127057. https://doi.org/10.1016/j.chemosphere.2020.127057

Xu S, Li JH, Yin ZB, Bian SY, Zhang YC (2020) A highly efficient strategy for enhancing the adsorptive and magnetic capabilities of biochar using Fenton oxidation. Bioresour Technol 315:123797. https://doi.org/10.1016/j.biortech.2020.123797

Yan LL, Kong L, Qu Z, Lo L, Shen GQ (2015) Magnetic biochar decorated with ZnS nanocrystals for Pb (II) removal. ACS Sustainable Chem Eng 3:125–132. https://doi.org/10.1021/sc500619r

Yang JP, Zhao YC, Ma SM, Zhu BB, Zhang JY, Zheng CG (2016) Mercury removal by magnetic biochar derived from simultaneous activation and magnetization of sawdust. Environ Sci Technol 50(21):12040–12047. https://doi.org/10.1021/acs.est.6b03743

Yang Y, Hu X, Zhao Y, Cui L, Huang Z, Long J, Xu J, Deng J, Wu C, Liao W (2017) Decontamination of tetracycline by thioureadioxide-reduced magnetic graphene oxide: effects of pH, ionic strength, and humic acid concentration. J Colloid Interface Sci 495:68–77. https://doi.org/10.1016/j.jcis.2017.01.075

Yi YQ, Huang ZX, Lu BZ, Xian JY, Tsang EP, Cheng W, Fang JZ, Fang ZQ (2019a) Magnetic biochar for environmental remediation: a review. Bioresour Technol 298:122468. https://doi.org/10.1016/j.biortech.2019.122468

Yi YQ, Tu GQ, Zhao DY, Tsang PE, Fang ZQ (2019b) Biomass waste components significantly influence the removal of Cr(VI) using magnetic biochar derived from four types of feedstocks and steel pickling waste liquor. Chem Eng J 360:212–220. https://doi.org/10.1016/j.cej.2018.11.205

Zhang H, Xue G, Chen H, Li X (2018) Magnetic biochar catalyst derived from biological sludge and ferric sludge using hydrothermal carbonization: preparation, characterization and its circulation in Fenton process for dyeing wastewater treatment. Chemosphere 191:64–71. https://doi.org/10.1016/j.chemosphere.2017.10.026

Zhang NQ, Yi YQ, Lian JT, Fang ZQ (2020) Effects of Ce doping on the Fenton-like reactivity of Cu-based catalyst to the fluconazole. Chem Eng J 395:124897. https://doi.org/10.1016/j.cej.2020.124897

Zhang QR, Wang JM, Lyu HH, Zhao Q, Jiang LS, Liu L (2019a) Ball-milled biochar for galaxolide removal: sorption performance and governing mechanisms. Sci Total Environ 659:1537–1545. https://doi.org/10.1016/j.scitotenv.2019.01.005

Zhang M, Gao B, Varnoosfaderani S, Hebard A, Yao Y, Inyang M (2013) Preparation and characterization of a novel magnetic biochar for arsenic removal. Bioresour Technol 130:457–462. https://doi.org/10.1016/j.biortech.2012.11.132

Zhang SJ, Ji YL, Dang J, Zhao JX, Chen SL (2019b) Magnetic apple pomace biochar: simple preparation, characterization, and application for enriching Ag(I) in effluents. Sci Total Environ 668:115–123. https://doi.org/10.1016/j.scitotenv.2019.02.318

Zhong DL, Zhang YR, Wang LL, Chen J, Jiang Y, Tsang DCW, Zhao ZZ, Ren SP, Liu ZH, Crittenden JC (2018) Mechanistic insights into adsorption and reduction of hexavalent chromium from water using magnetic biochar composite: key roles of Fe_3O_4 and persistent free radicals. Environ Pollut 243:1302–1309. https://doi.org/10.1016/j.envpol.2018.08.093

Zhou XH, Liu YC, Zhou JJ, Guo J, Ren JL, Zhou F (2018) Efficient removal of lead from aqueous solution by urea-functionalized magnetic biochar: preparation, characterization and mechanism study. J Taiwan Inst Chem E 91:457–467. https://doi.org/10.1016/j.jtice.2018.04.018

Zhou Z, Liu YG, Liu SB, Liu HY, Zeng GM, Tan XF, Yang CP, Ding Y, Yan ZL, Cai XX (2017) Sorption performance and mechanisms of arsenic(V) removal by magnetic gelatin-modified biochar. Chem Eng J 314:223–231. https://doi.org/10.1016/j.cej.2016.12.113

Zhuang ZC, Wang L, Tang JC (2021) Efficient removal of volatile organic compound by ball-milled biochars from different preparing conditions. J Hazard Mater 406:124676. https://doi.org/10.1016/j.jhazmat.2020.124676

Zou HW, Zhao JW, He F, Zhong Z, Huang JS, Zheng YL, Zhang Y, Yang YC, Yu F, Bashir MA, Gao B (2021) Ball milling biochar iron oxide composites for the removal of chromium (Cr(VI)) from water: performance and mechanisms. J Hazard Mater 413:125252. https://doi.org/10.1016/j.jhazmat.2021.125252